Geomechanics and Engineering, *Vol. 17, No. 6 (2019) 553-564*
DOI: https://doi.org/10.12989/gae.2019.17.6.553

Experimental study on rock-concrete joints under cyclically diametrical compression

Xu Chang*[1], Tengfei Guo[1], Jianyou Lu[2] and Hui Wang[1]

[1]*School of Civil Engineering, Henan Polytechnic University, Jiaozuo, China*
[2]*China Construction Shenzhen Decoration Co., Ltd, China*

(Received December 29, 2018, Revised February 21, 2019, Accepted March 17, 2019)

Abstract. This paper presents experimental results of rock-concrete bi-material discs under cyclically diametrical compression. It was found that both specimens under cyclical and static loading failed in three typical modes: shear crack, tensile crack and a combined mode of shear and wing crack. The failure modes transited gradually from the shear crack to the tensile one by increasing the interface angle between the interface and the loading direction. The cycle number and peak load increased by increasing the interface angle. The number of cycles and peak load increased with the interface groove depth and groove width, however, decreased with increase in interface groove spacing. The concrete strength can contribute more to the cycle number and peak load for specimens with a higher interface angle. Compared with the discs under static loading, the cyclically loaded discs had a lower peak load but a larger deformation. Finally, the effects of interface angle, interface asperity and concrete strength on the fatigue strength were also discussed.

Keywords: rock-concrete disc; cyclic loading; crack patterns; nominal tensile strength

1. Introduction

The joints between rock foundations and concrete retaining structures can be commonly found in dams, retaining walls and shotcrete structures in tunneling and underground mining (Komurlu *et al*. 2015, Erarslan and Williams 2012a, b, Granrut *et al.* 2019, Fishman 2009a, b, Bahaaddini *et al.* 2016, Baak *et al.* 2017, Jayakody *et al.* 2014). The rock-concrete joints play a critical role in the composite structures by providing effective load transfer between rocks and concrete and keeping structure integrity and durability. On the other hand, the rock-concrete joints are considered as the weak link for these structures, which can highly influence the overall structure stability. Therefore, understanding of the failure mechanism of rock-concrete joints is of importance for the rock-concrete composite structures.

Many experiments, numerical and theoretical analysis have been carried out to investigate the rock-concrete joints. The effects of interface asperity on the shear performances were investigated by shear tests (Zhu *et al*. 2010, Zhao *et al*. 2018, Kodikara 1989) and indicated that the regular interface had a higher shear resistance than the irregular asperities. Andjeikovic *et al.* (2015) also tested the rock-concrete joints with different rocks. The results showed that the parameters of rocks determined the failure and deformations. Yang and Deeks (2007) tested the fracture toughness of rock-concrete joints by the rock-concrete beams with a single-notch. Their results indicated that the interface fracture toughness was close related to the mode mixity ratio.

The rock-concrete joints always experience dynamic loading and cyclic loading induced by blasting, earthquakes, vehicles through the tunnel and excavation engineering (Bagde and Petrosˇ 2005a, b, 2009, Sukplum and Wannakao 2016). These loading conditions may greatly affect the mechanical performances of rock-concrete joints. It is therefore important to investigate the behaviour of rock-concrete joints under cyclic loading.

Significant efforts have been devoted to investigation of the rock joints under cyclic loading both in tests and theoretical analyses. The cyclic shear test was one representative method to assess the mechanical behavior of rock joints. The artificial joints with different shapes were also tested (Dong *et al.* 2017, Liu *et al.* 2017a, Chang *et al*. 2018). Liu *et al.* (2018) further tested the loading parameters on the mechanical performances of rock joints. Some sophisticated models have been developed to represent the mechanical behaviour of the joints. Liu *et al*. (2017b) proposed the interlock-friction model for dynamic shear response. Plesha (1987) and Qiu *et al.* (1993) also proposed different empirical models for rock joints under cyclic loading. These studies have contributed to a better understanding of the behaviour of rock joints, which has in turn led to higher quality designs and safety improvements. They are also fundamental to further investigate the rock-concrete joints under cyclic loading.

For a rock-concrete joint, three different parts should be included, the rock, concrete and interface between them. In fact, most of the existing studies focus on the mechanical behaviour of the rock-concrete interface under compression/shear stress conditions. The implicit assumption is that failures of the rock-concrete structure are determined only by the rock-concrete interface. The authors

*Corresponding author, Professor
E-mail: changxu1980@hpu.edu.cn

http://www.techno-press.org/?journal=gae&subpage=7
ISSN: 2005-307X (Print), 2092-6219 (Online)

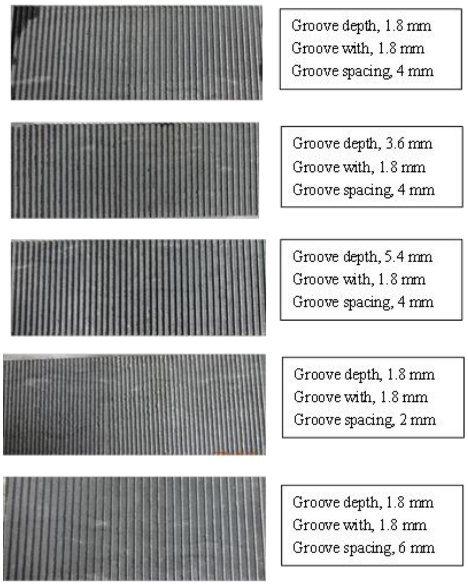

(a) Preparation for joint interface

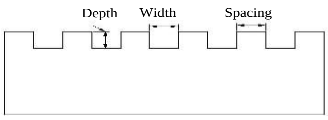

(b) Interface asperity

Fig. 1 Roughening of rock portion at the interface

(a) Core drilling

(b) Test specimen after machining

Fig. 2 Procedure for specimen preparation

believe that the stability of rock/concrete structures is related to not only the interface properties but also overall behaviour, including the interface, rock and concrete material. However, the overall behaviour of the rock-concrete structures is seldom considered in the existing studies. This study therefore considers the interface, rock and concrete as a bi-material and tries to investigate its overall behaviour under cyclically diametrical compression.

2. Experimental setup

2.1 Test specimens

In practice, the rock surfaces were always drilled and flushed before casting the concrete to enhance the interface performances. In this paper, the rock surfaces were also roughened by introducing different grooves, as presented in Fig.1. After curing in the same conditions for 28 days, the specimens were carefully cored so that the rock-concrete interfaces coincided with disc diameter and then machined to the desired dimensions. The sizes of specimens were 50 mm (diameter, d) and 25 mm (height, t) (ISRM, 1978) with errors within ±0.5 mm, and the parallelism of the specimen ends within ±0.1 mm, as shown in Fig. 2). 14 series of specimens were prepared (A series, B series and N series), as listed in Table 1. For comparing purpose, the rock-concrete discs under static loading were also tested. These specimens were denoted by their loading condition. For example, specimen DA1 and SA1 meant that both

Table 1 Test specimens

Specimen	α	Groove(Depth×Width×Spacing, mm)	*NS*(MPa)	*NS*(MPa)	σ_c (MPa)	σ_t (MPa)	E_c(GPa)	v_c
A1	0°	1.8×1.8×4	0.36	0.11	41.30	2.93	16.52	0.213
A2	15°	1.8×1.8×4	1.02	0.72	41.30	2.93	16.52	0.213
A3	30°	1.8×1.8×4	2.35	1.35	41.30	2.93	16.52	0.213
A4	45°	1.8×1.8×4	3.08	2.96	41.30	2.93	16.52	0.213
A5	60°	1.8×1.8×4	3.20	2.89	41.30	2.93	16.52	0.213
A6	75°	1.8×1.8×4	3.54	2.97	41.30	2.93	16.52	0.213
A7	90°	1.8×1.8×4	3.30	2.43	41.30	2.93	16.52	0.213
B1	*0°*	1.8×1.8×4	0.82	0.19	55.30	3.78	17.30	0.196
B2	15°	1.8×1.8×4	1.28	0.37	55.30	3.78	17.30	0.196
B3	30°	1.8×1.8×4	2.14	1.88	55.30	3.78	17.30	0.196
B4	45°	1.8×1.8×4	3.22	2.85	55.30	3.78	17.30	0.196
B5	60°	1.8×1.8×4	3.77	3.92	55.30	3.78	17.30	0.196
B6	75°	1.8×1.8×4	3.92	3.88	55.30	3.78	17.30	0.196
B7	90°	1.8×1.8×4	3.94	4.40	55.30	3.78	17.30	0.196
C1	0°	1.8×1.8×4	0.32	0.21	77.50	3.72	19.09	0.227
C2	15°	1.8×1.8×4	0.16	1.16	77.50	3.72	19.09	0.227
C4	45°	1.8×1.8×4	1.95	2.90	77.50	3.72	19.09	0.227
C7	90°	1.8×1.8×4	3.33	4.05	77.50	3.72	19.09	0.227
D1	0°	3.6×1.8×4	0.39	0.52	41.30	2.93	16.52	0.213
D2	15°	3.6×1.8×4	0.98	1.16	41.30	2.93	16.52	0.213
D3	30°	3.6×1.8×4	2.85	1.82	41.30	2.93	16.52	0.213
D4	45°	3.6×1.8×4	3.02	2.38	41.30	2.93	16.52	0.213
D5	60°	3.6×1.8×4	3.10	2.51	41.30	2.93	16.52	0.213
D6	75°	3.6×1.8×4	2.71	2.98	41.30	2.93	16.52	0.213
D7	90°	3.6×1.8×4	3.05	3.44	41.30	2.93	16.52	0.213
E1	0°	3.6×1.8×4	0.45	0.10	55.30	3.78	17.30	0.196
E2	15°	3.6×1.8×4	1.55	1.24	55.30	3.78	17.30	0.196
E3	30°	3.6×1.8×4	1.73	2.13	55.30	3.78	17.30	0.196
E4	45°	3.6×1.8×4	3.56	2.24	55.30	3.78	17.30	0.196
E5	60°	3.6×1.8×4	3.41	2.44	55.30	3.78	17.30	0.196
E6	75°	3.6×1.8×4	3.72	2.36	55.30	3.78	17.30	0.196
E7	90°	3.6×1.8×4	3.86	2.42	55.30	3.78	17.30	0.196
F1	0°	3.6×1.8×4	0.36	0.35	77.50	3.72	19.09	0.227
F2	15°	3.6×1.8×4	1.37	0.64	77.50	3.72	19.09	0.227
F3	30°	3.6×1.8×4	2.65	0.83	77.50	3.72	19.09	0.227
F4	45°	3.6×1.8×4	3.43	2.39	77.50	3.72	19.09	0.227
F5	60°	3.6×1.8×4	4.00	3.87	77.50	3.72	19.09	0.227
F6	75°	3.6×1.8×4	4.05	3.90	77.50	3.72	19.09	0.227
F7	90°	3.6×1.8×4	3.56	4.48	77.50	3.72	19.09	0.227
G1	0°	5.4×1.8×4	0.32	0.17	41.30	2.93	16.52	0.213
G2	15°	5.4×1.8×4	1.03	1.83	41.30	2.93	16.52	0.213
G3	30°	5.4×1.8×4	1.79	1.88	41.30	2.93	16.52	0.213
G4	45°	5.4×1.8×4	2.55	2.44	41.30	2.93	16.52	0.213
G5	60°	5.4×1.8×4	2.99	2.89	41.30	2.93	16.52	0.213
G6	75°	5.4×1.8×4	3.10	2.96	41.30	2.93	16.52	0.213
G7	90°	5.4×1.8×4	2.94	2.99	41.30	2.93	16.52	0.213

Table 1 Continued

Specimen	α	Groove(Depth×Width×Spacing, mm)	*NS*(MPa)	*NS*(MPa)	σ_c (MPa)	σ_t (MPa)	E_c (GPa)	v_c
H1	0°	5.4×1.8×4	0.03	0.19	55.30	3.78	17.30	0.196
H2	15°	5.4×1.8×4	0.45	2.35	55.30	3.78	17.30	0.196
H3	30°	5.4×1.8×4	2.77	2.41	55.30	3.78	17.30	0.196
H4	45°	5.4×1.8×4	2.78	2.43	55.30	3.78	17.30	0.196
H5	60°	5.4×1.8×4	2.94	2.91	55.30	3.78	17.30	0.196
H6	75°	5.4×1.8×4	3.67	3.47	55.30	3.78	17.30	0.196
I1	0°	5.4×1.8×4	0.40	0.62	77.50	3.72	17.30	0.196
I2	15°	5.4×1.8×4	1.09	1.22	77.50	3.72	19.09	0.227
I3	30°	5.4×1.8×4	2.70	1.40	77.50	3.72	19.09	0.227
I4	45°	5.4×1.8×4	2.86	1.49	77.50	3.72	19.09	0.227
I5	60°	5.4×1.8×4	2.85	3.53	77.50	3.72	19.09	0.227
I6	75°	5.4×1.8×4	3.48	2.48	77.50	3.72	19.09	0.227
I7	90°	5.4×1.8×4	4.08	3.40	77.50	3.72	19.09	0.227
J1	0°	1.8×1.8×2	1.06	0.54	55.30	3.78	19.09	0.227
J2	15°	1.8×1.8×2	0.92	2.89	55.30	3.78	17.30	0.196
J3	30°	1.8×1.8×2	2.73	2.45	55.30	3.78	17.30	0.196
J4	45°	1.8×1.8×2	3.19	2.99	55.30	3.78	17.30	0.196
J5	60°	1.8×1.8×2	3.68	4.30	55.30	3.78	17.30	0.196
J6	75°	1.8×1.8×2	3.54	4.55	55.30	3.78	17.30	0.196
J7	90°	1.8×1.8×2	3.48	4.73	55.30	3.78	17.30	0.196
K1	0°	1.8×1.8×6	1.42	0.13	55.30	3.78	17.30	0.196
K4	45°	1.8×1.8×6	2.30	2.87	55.30	3.78	17.30	0.196
K7	90°	1.8×1.8×6	3.25	3.93	55.30	3.78	17.30	0.196
L1	*0°*	3.6×3.6×4	1.01	1.33	55.30	3.78	17.30	0.196
L2	15°	3.6×3.6×4	1.95	1.83	55.30	3.78	17.30	0.196
L3	30°	3.6×3.6×4	2.60	2.96	55.30	3.78	17.30	0.196
L4	45°	3.6×3.6×4	3.09	2.92	55.30	3.78	17.30	0.196
L5	60°	3.6×3.6×4	3.02	3.40	55.30	3.78	17.30	0.196
L6	75°	3.6×3.6×4	3.46	3.91	55.30	3.78	17.30	0.196
L7	90°	3.6×3.6×4	3.03	2.59	55.30	3.78	17.30	0.196
M1	0°	3.6×5.4×4	1.35	1.78	55.30	3.78	17.30	0.196
M2	15°	3.6×5.4×4	1.51	1.12	55.30	3.78	17.30	0.196
M3	30°	3.6×5.4×4	1.82	2.96	55.30	3.78	17.30	0.196
M4	45°	3.6×5.4×4	2.93	2.42	55.30	3.78	17.30	0.196
M5	60°	3.6×5.4×4	3.59	1.80	55.30	3.78	17.30	0.196
M6	75°	3.6×5.4×4	3.62	3.48	55.30	3.78	17.30	0.196
M7	90°	3.6×5.4×4	3.49	2.41	55.30	3.78	17.30	0.196
N1	0°	3.6×1.8×2	1.19	0.27	55.30	3.78	17.30	0.196
N2	15°	3.6×1.8×2	2.26	1.74	55.30	3.78	17.30	0.196
N3	30°	3.6×1.8×2	3.29	1.34	55.30	3.78	17.30	0.196
N4	45°	3.6×1.8×2	3.22	1.38	55.30	3.78	17.30	0.196
N5	60°	3.6×1.8×2	3.04	1.89	55.30	3.78	17.30	0.196
N6	75°	3.6×1.8×2	3.22	2.88	55.30	3.78	17.30	0.196
N7	90°	3.6×1.8×2	3.81	2.94	55.30	3.78	17.30	0.196

specimens had the same parameters except the former was under cyclic loading and the latter was under static loading.

2.2 Materials properties

The limestones were used and the elastic modulus,

Table 2 Concrete mixes

Mix proportion by weight (Cement：sand：gravel：water)	σ_c (MPa)	$s_{\sigma c}$	σ_t (MPa)	$s_{\sigma t}$	E_c (GPa)	s_{Ec}	v_c	s_{vc}
1:0.55:1.15:0.50	41.30	0.11	2.93	0.08	16.52	0.13	0.176	0.08
1:0.63:0.95:0.40	55.30	0.14	3.72	0.13	17.30	0.10	0.223	0.10
1:0.92:0.88:0.32	77.50	0.09	3.78	0.10	19.09	0.11	0.151	0.09

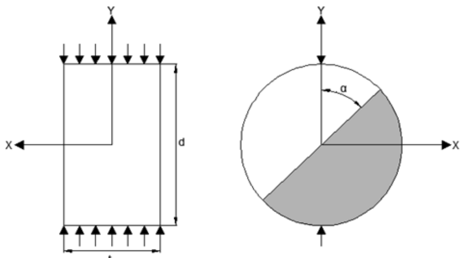

Fig.3 Sketch for the test specimen. ranges from 0º to 90º

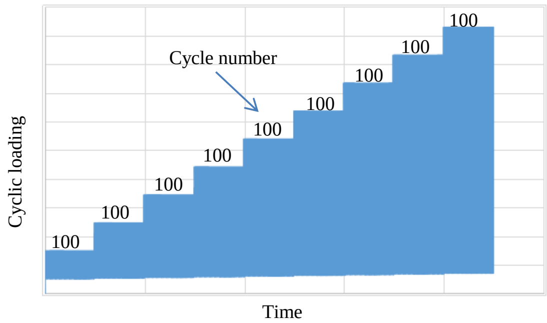

(a) Sketch for load-cycle number relationship

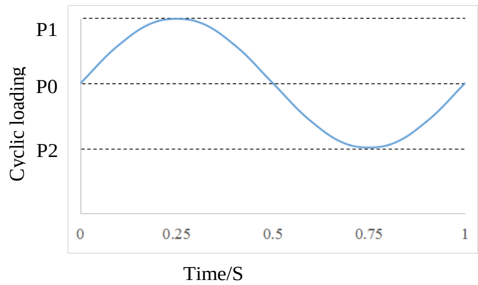

(b) A loading cycle

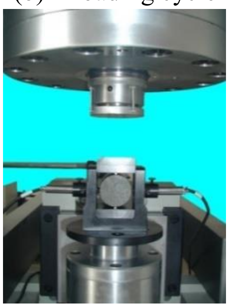

(c) Test specimen

Fig. 4 Test arrangement

compressive strength, tensile strength and Poisson's ratio were 66.98 GPa, 170.40 MPa, 5.35 MPa and 0.347, respectively. Three types of concretes (Table 1) were adopted and the average values for compressive strength (s_c), tensile strength (s_t), elastic modulus (E_c) and Poisson's ratio (v) of these concretes were summarized in Table 2. ss_c, ss_t, s_{Ec}, s_v were the standard deviations for s_c, s_t, E_c and v, respectively.

2.3 Materials properties

In the Brazilian test, a disc was compressed by two opposite lines. Tensile stresses were induced along the loading plane. As a result, a tensile fracture can also be formed along the loading plane. However, for the specimens in this study, the interface between rock and concrete would be in different stress sates, ranging from tension, shear and compression by selecting the different interface angle (a), which was the angle between the interface and the loading direction, as indicated in Fig. 3. Different values for the interface angle (a=0º, 15º, 30º, 45º, 60º, 75º, 90º) were tested. In this study, a step cyclic loading was adopted and the number of cycles for each loading step is 100, as presented in Fig. 4(a). For a given load step, the sinusoidal cyclic loading was applied (Fig. 4(b)). The minimum load (P2) was maintained constant at 0.5 kN to ensure the disc ends remained in contact with the loading plates during the test. P1 for first step was 1.0 kN and then increased by 1.0kN a step until failure of the specimen. All specimens were tested under a servo-controlled testing machine. Fig. 4(c) gave a general view of the test setup. Two linear variable differential transformers (LVDTs) were adopt to obtain the displacements. The applied loading frequency is 1.0 Hz.

3. Test results

3.1 Materials properties

The test results indicated that the failure modes of the rock-concrete discs were dependent on the interface angle. The typical failure modes were presented in Fig. 5. For a lower interface angle, the specimen under static loading was split by a crack along the interface (shear crack). As further increasing the angle to a moderate angle, the specimen failed in a combined pattern of cracking along the interface (shear crack) and cracking in the matrix (wing crack). If the interface angle increased to a higher value, the specimen was split by the crack in diameter direction (tensile crack). For the extreme case of a=0º, the specimen also failed by a crack along the interface. However, the interface crack for a=0º was a tensile crack because the interface was in tension. For specimens under cyclic loading, the similar crack modes can be observed with increase in the interface angle.

It can be further found that the shear crack lengths (denoted as l_i in Fig. 6) for static and cyclic loading were quietly different. To describe the crack modes more quantitatively, the shear crack ratio (j) was defined as follows

$$\varphi = \frac{l_i}{d} \tag{1}$$

where d was the diameter of test disc.

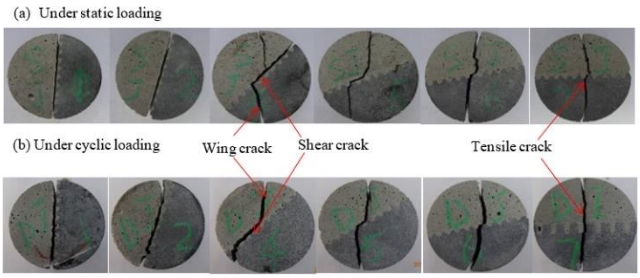

Fig. 5 Typical failure modes varied as a function of interface angle (a=0°, 15°, 45°, 60°, 75°, 90°)

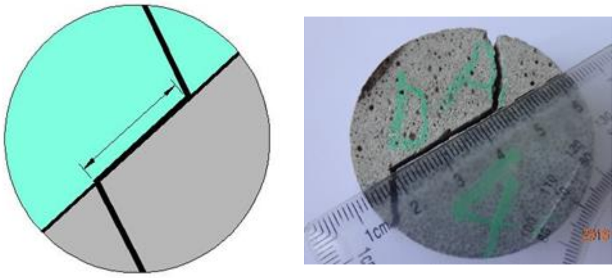

Fig. 6 Measure shear crack length ratio

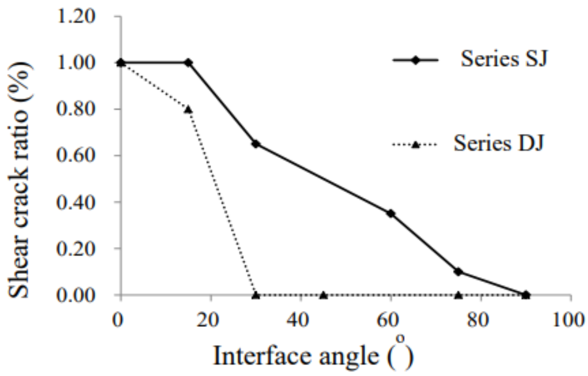

(a)

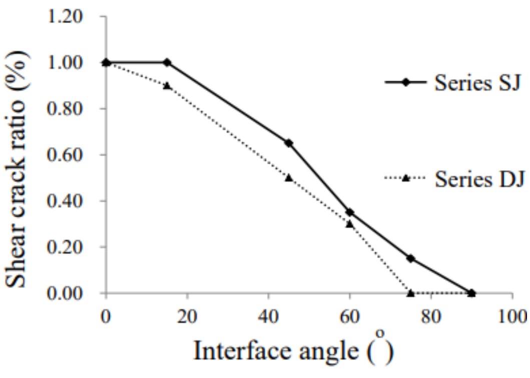

(b)

Fig. 7 Shear crack ratio for different failure modes

Obviously, j=1meant the specimen failed by shear crack (the extreme case of a=0° was not included) and j=0 indicated the specimen failed by tensile crack. For the combined mode, j=1 ranged between 0 and 1 ($0<j<1$).

The shear crack ratio versus interface angle for specimens under static loading and cyclic loading were presented in Fig. 7. It can be seen from Fig. 7(a) that, for specimens under static loading, the ratio j was 1.0 for a=15°. As the angle a reached 30°, the ratio j dropped to 0.65. And then the ratio j dropped to zero at a=90°. For specimens under cyclic loading, ratio j dropped to 0.85 at a=15°. The ratio j dropped to zero rapidly at a=30° and kept zero as further increasing the angle. According to Fig. 7(b), the ratio j for specimen under static loading also began to decrease at a=15°. As the angle ranged from a=30° to a=75°, the statically loaded specimen failed in the combined mode. However, the cyclically loaded specimen failed in the combined mode as the angle increased from a=15° to a=30°. One can conclude that the cyclically loaded specimen would begin to fail in a combined mode at a lower interface angle. With the same interface angle, the shear crack ratio for the specimen under cyclic loading was smaller than that under static loading. This indicated the gradual deterioration of the interfacial properties under cyclic loading, which resulted in the larger shear crack ratio.

3.2 Load-deformation curves

The applied load, total cycles and envelope line for each loading step were monitored for each tested specimen and the typical load-deformation curves were presented in Figs. 8-11.

The effects of interface angle on the load-deformation curves for discs under cyclic loading were presented in Fig. 8. It can be seen that the specimen (Fig. 8(a)) with a=15° failed after only 101 loading cycles at the peak load of 0.8 kN. As the angle increased up to a=30°, the specimen (Fig. 8(b)) failed after 304 loading cycles and the peak load increased up to 3.8 kN. As further increasing the angle to a=60° (Fig. 8(c)), the number of loading cycles and the peak load were 718 kN and 7.9 kN, respectively. For cases of a=75° (Fig. 8(d)), the number of loading cycles and peak load were 748 and 7.8 kN. As the angle increased to the maximum value of a=90° (Fig. 8(e)), the number of loading cycles and the peak load reached the maximum values of 847 and 8.4 kN, respectively. Fig. 8(f) revealed the relationship between the loading cycles and the interface angle. It can be seen that the number of loading cycles increased by increasing the interface angle. This further indicated that fatigue behavior of the rock-concrete disc was close related to the crack modes. If the specimen was cracked along the weaker interface (a=15°), the number of loading cycles was lower. As further increasing the angle (a=30°, a=60°), the specimens failed in the combined mode and the crack propagated partly along the weak interface. As a result, the number of loading cycles increased. If the specimen failed by tensile crack that propagated completely in the concrete and rock (a=90°), the interface cannot further weaken the mechanical performances of the specimen. As a result, the number of loading cycles reached the maximum value.

The effects of the concrete strength on the load-deformation curves were presented in Fig. (9). Three groups of specimens (group 1:DB1 and DC1, group 2: DE4 and DF4, group 3: DE7 and DF7) were discussed. For each group, both specimens had the same material parameters and interface asperity except that the concrete strengths

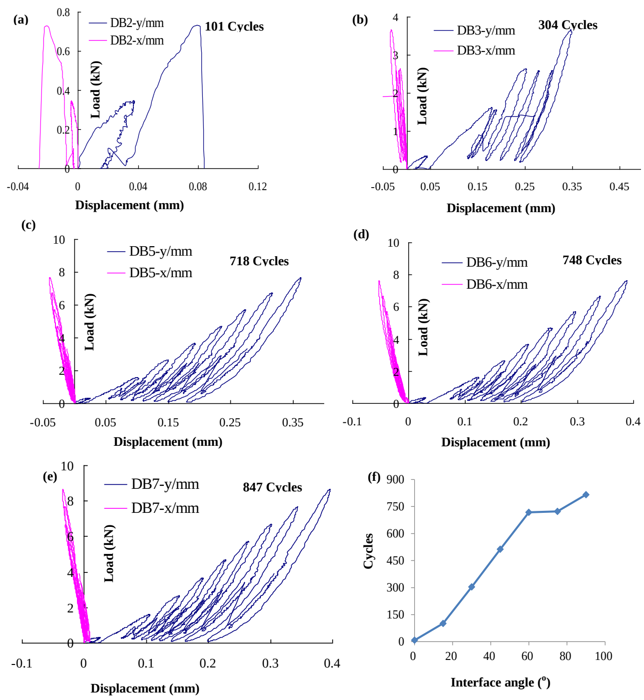

Fig. 8 Effect of interface angle on load-deformation curves (envelope lines for loading steps)

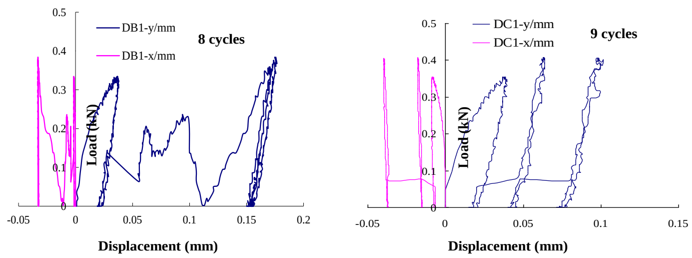

(a) Interface angle a=0°

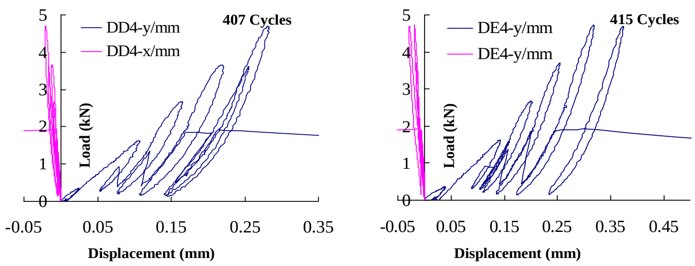

(b) Interface angle a=45°

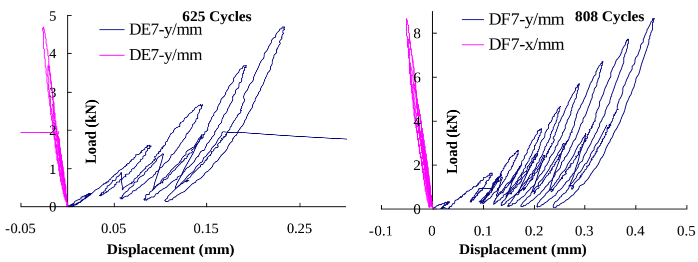

(c) Interface iangle a=90°

Fig. 9 Effect of concrete strength on load-displacement curves (envelope lines for loading steps)

were 55.3 MPa and 77.5 MPa, respectively. It can be seen from Fig. 9(a) that, at a lower interface angle of a=0°, the cycle number and peak for both specimens were almost same even though the concrete strengths for them were quite different. As the interface angle increased to a=15°, the differences in the cycle number and peak load were not

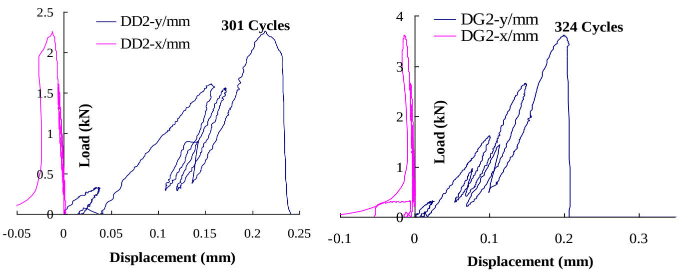

(a) Effect of groove depth(depth for specimen DD2=3.6 mm, depth for specimen DG2=5.4 mm

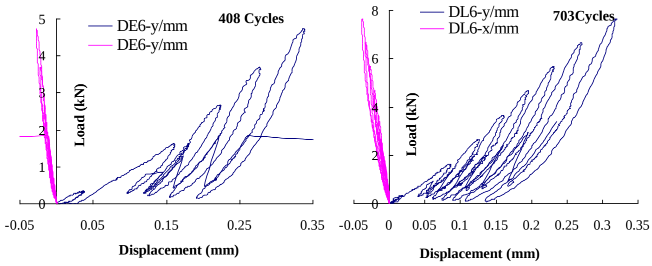

(b) Effect of groove width (width for specimen DE6=1.8 mm, with for specimen DL6=3.6 mm)

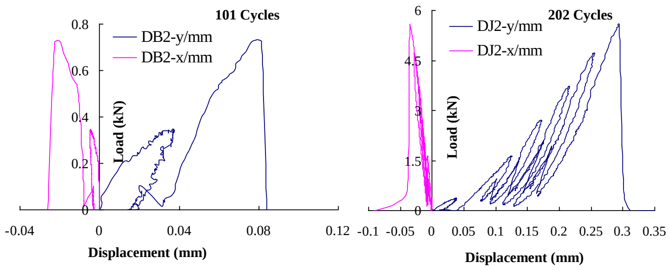

(c) Effect of groove spacing

Fig. 10 Effect of concrete strength on load-displacement curves (envelope lines for loading steps)

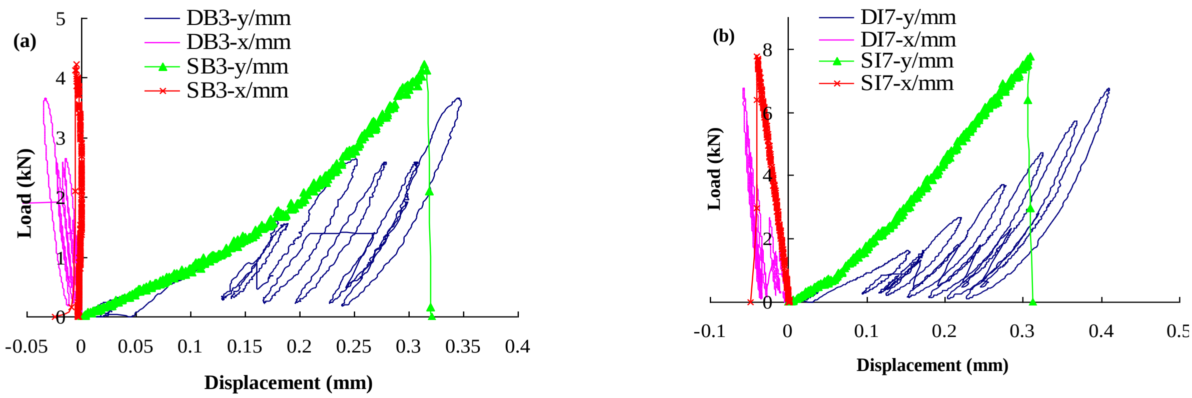

Fig. 11 Comparison of load-deformation curves between cyclic loading (envelope lines for loading steps) and static loading

yet obvious, as illustrated in Fig. 9(b). The load-deformation curves were compared in Fig. 9(c) for a higher interface angle of a=90º. For specimen with a lower concrete strength of 55.3 MPa, the number of loading cycles and peak load were 454 kN and 4.9 kN, respectively. As the concrete strength increased to 77.5 MPa, the number of loading cycles and peak load increased to 808 kN and 8.2 kN, respectively. It was indicated that the concrete strength can obviously affect the load-deformation curves of cyclically loaded specimens only at a high interface angle.

Fig .10 presented the effects of interface asperity on the load-deformation curve. It can be seen that the number of loading cycles and peak load increased by increasing the groove depth, as illustrated in Fig. 10(a). Fig. 10(b) revealed that the number of loading cycles and peak load increased by increasing the groove width. However, the number of loading cycle and peak load decreased by increasing the groove spacing, as shown in Fig.10(c).

The load-deformation curves under static loading were presented in Fig. 11 for comparing purpose. It can be seen that the peak load under cyclic loading was lower than that under static loading, whereas the displacements under cyclic loading were greater than those under static loading. This indicated that the gradual deterioration of the interface

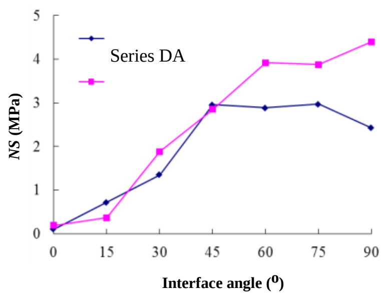

Fig. 12 Effect of concrete strength on *NS*

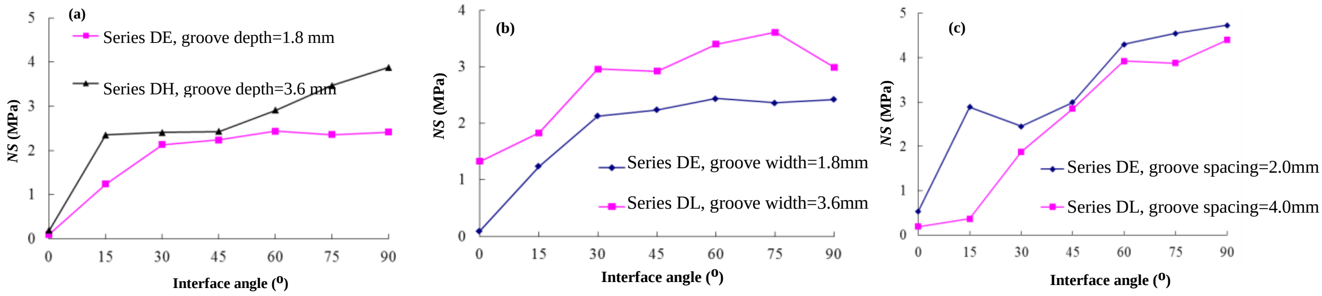

Fig. 13 Effects of interface asperity. (a) effects of groove depth, (b) effects of groove width and (c) effects of groove spacing

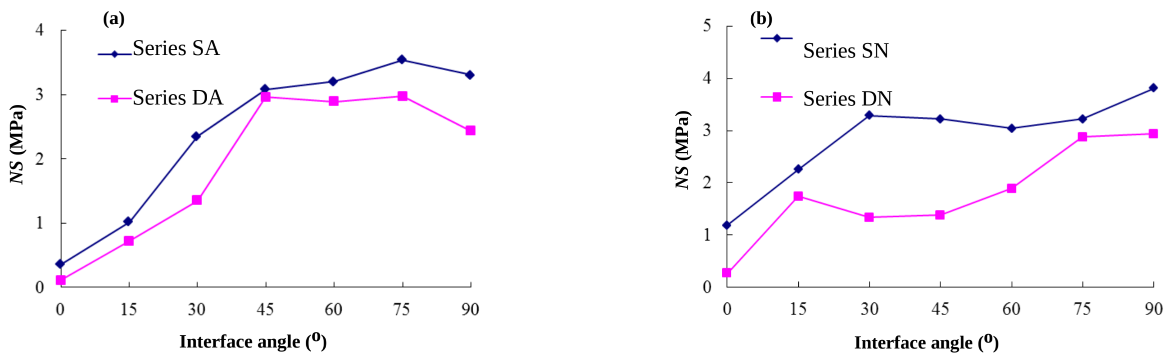

Fig. 14 Comparison of *NS* between specimens under cyclic loading and static loading

properties under cyclic loading can reduce the bearing capacity of the bi-material and increase the deformability.

3.3 Fatigue strength

Following the ISRM suggestion (1978) for the standardized of the Brazilian-disc test, all the specimens were loaded by two steel wires to ensure the specimens were under diametral compression. The indirect tensile strength (*S*) for the disc under Brazilian test condition can be generally described as

$$S = \frac{2P_{\max}}{\pi dt} \tag{2}$$

where the P_{max} was the peak value during the load process. d and t were the diameter and thickness for the disc, respectively. This formula was certainly considered for an isotropic rock or concrete material. One of the important characteristics was that the disc fails by a typical vertical fracture in the loading direction. Since the discs from rock-concrete bi-material always failed by a combined pattern, it was inappropriate to determine the tensile strength straightforward by Eq (2). In this study, this formula was also adopted just for comparison purposes and *S* was therefore named nominal tensile strength (*NS*). The *NS* for all the test specimens under both cyclic and static loadings were listed in Table 1.

Fig. 12 gave the effects of concrete strength on *NS*, where two series of test discs were included and for each series, the discs had the same dimension, materials parameters and interface asperity. The concrete strengths for series DA and DB were 41.3 MPa and 55.3 MPa, respectively. It can be seen from the figures that the differences in *NS* between the two series were very small for $a \le 45°$. For $a \ge 45°$, the *NS* for specimen in series DB was higher than that in series DA at a given interface angle. It was indicated that the concrete strength can contributed more to the *NS* at a higher interface angle. It can be also seen that, for each series, the *NS* increased by increasing the interface angle.

Fig. 13 showed the typical curve of effects of interface asperity on the *NS*. It can be seen from the Fig. 13(a) that, at a given interface angle, the specimen in series DH had a higher *NS* than that in DE series. Fig. 13(b) revealed that a

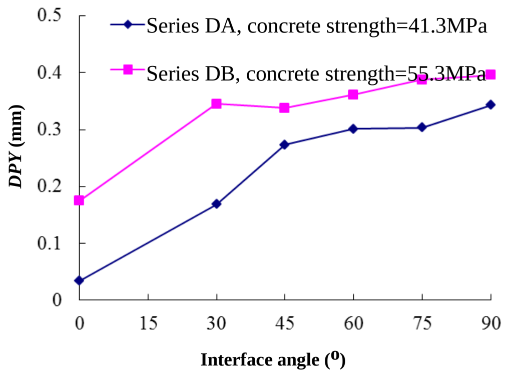

Fig. 15 Effects of concrete strength on *DPY*

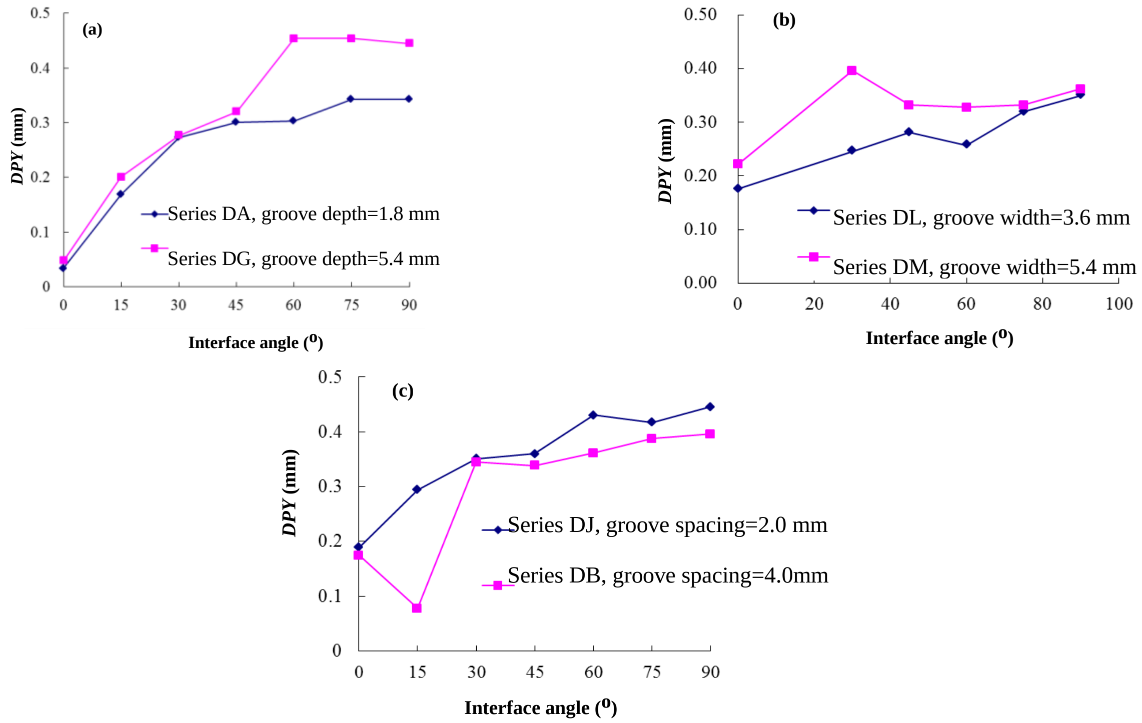

Fig. 16 Effects of interface asperity on *DPY*.(a) effects of groove depth, (b) effects of groove width and (c) effects of groove spacing

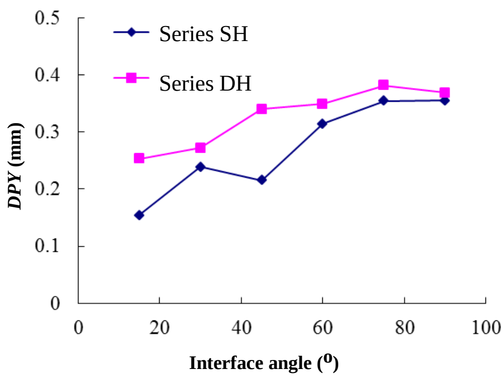

Fig. 17 Comparison of DPY between specimens under cyclic loading and static loading

wider groove can lead to a higher *NS*. The effects of groove spacing were presented in Fig. 13(c). At a given interface angle, the specimen in series DJ had higher *NS* value than specimen in series DB.

The *NS* values for specimens both under static loading and cyclic loading were compared in Fig. 14. It can be seen that the *NS* value increased by increasing interface angle. However, with the same interface angle, the *NS* value for specimen under cyclic loading was lower than that under static loading.

3.4 Deformation

In this section, the displacement at peak load in y direction (*DPY*) was adopted to discuss the deformation behaviour of a specimen under cyclic loading. Fig. 15 indicated the *DPY* increased with the increasing of interface angle. With the same interface angle, a higher concrete strength can lead to a greater *DPY*. Fig. 16(a) presented the effects of groove depth on the *DPY*. At a given angle, the specimen with a greater groove depth had a higher *DYP*.

Fig. 16(b) indicated that the *DYP* increased by increasing the groove width. Fig. 16(c) indicated that the specimen with lower groove spacing had a higher *DPY*. The *DPY* values for specimens under static loading (series SH) and those under cyclic loading (series DH) were compared in Fig. 17. For both series, the *DPY* value increased with the increasing of interface angle. At a given interface angle, the *DPY* value under cyclic loading was higher than that under static loading.

4. Conclusions

The primary aim of this paper is to investigate the overall behaviour of rock/concrete disc, including rock, concrete and interaction between rock and concrete. More attentions are paid on the parameters related to the bi-material interface, including interface angle and interface asperity. In the disc configuration adopted in this paper, the interface experienced various stress sates, tension, shear and compression by selecting the interface angle. As a result, the disc failed by various patterns, tension, shear and the combined pattern of shear and wing crack. The mechanical performances of rock-concrete structures were related to not only the interface properties but also the material properties of rock and the concrete. Therefore, the fracture mechanism for rock-concrete bi-material was more complex than the shear mechanism of joints under shear, where only interface behaviour was always considered (Dong *et al.* 2017, Chang *et al*. 2018, Yang *et al.* 2001, Asadi *et al.* 2012).

This paper was just an attempt to explore the complex mechanical performances of rock-concrete bi-material discs under cyclically diametrical compression and more investigations should be further conducted in future. And following conclusions can be drawn based on this limited study:

(1) For rock-concrete bi-material discs under both cyclic and static loading, three typical crack modes can be observed: tension crack, shear crack and the combined mode of shear and wing crack. Various crack modes can be achieved by selecting the interface angle between the interface and loading direction. The shear crack ratio was defined to quantitatively describe the crack modes. It was further found that the specimen under cyclic loading would fail by a combined mode at a lower interface angle compared with the specimen under static loading. At a given interface value, the shear crack ratio for the specimen under cyclic loading was smaller than that under static loading.

(2) The interface angle, interface asperity and concrete strength had important effects on the load-deformation curves of rock-concrete discs under cyclically diametrical compression. The cycle number and peak load increased by increasing the interface angle. The number of cycle and peak load increased by increasing interface groove depth and groove width, however, both decreased by increasing interface groove spacing. The concrete strength can contribute more to the cycle number and to peak load at a higher interface angle.

(3) The *NS* and *DPY* were close related to the interface angle, interface asperity and concrete strength. Generally, the *NS* and *DPY* increased by increasing the interface angle. The *NS* and *DPY* increased by increasing the interface groove depth and width. However, they decreased with the increasing of groove spacing. Compared with the specimen under static loading, the cyclically loaded specimen had a lower *NS* but a higher *DPY*.

Acknowledgements

The work described in this paper was fully supported by National Natural Science Fund of China Project No. 51674100) and the Program for Science and Technology Innovation Talents Universities of Henan Province (Project No. 18HASTIT017)

References

Andjeikovic, V., Pavlovic, N., Lazarevic, Z. and Nedovic, V. (2015), "Modelling of shear characteristics at the concrete-rock mass interface", *Int. J. Rock Mech. Min. Sci*., **76**, 222-236.

Asadi, M.S., Rasouli, V. and Barla, G. (2012), "A bonded particle model simulation of shear strength and asperity degradation for rough rock fractures", *Rock Mech. Rock Eng.*, **45**(5), 649-75.

Baak, S.H., Cho, G.C. and Song, K.I. (2017), "Stability analysis on the concrete slab of the highest concrete-faced rock-fill dam in South Korea", *Geomech. Eng.*, **13**(5), 881-892.

Bagde, M.N. and Petroš, V. (2005a), "Waveform effect on fatigue properties of intact sand stone in uniaxial cyclical loading", *Rock Mech. Rock Eng*., **38**(3), 169-196

Bagde, M.N. and Petroš, V. (2005b), "Fatigue properties of intact sand stone samples subjected to dynamic uniaxial cyclical loading", *Int. J. Rock Mech. Min. Sci*., **4**(2), 237-250

Bagde, M.N. and Petroš, V. (2009), "Fatigue and dynamic energy behaviour of rock subjected to cyclical loading", *Int. J. Rock Mech. Min. Sci*., **46**, 200-209

Bahaaddini, M., Hagan, P.C., Mitra, R. and Khosravi, M.H. (2016), "Experimental and numerical study of asperity degradation in the direct shear test", *Eng. Geol*., **204**, 41-52.

Chang, X., Lu, J., Wang, S. and Wang, S. (2018), "Mechanical performances of rock-concrete bi-material disks under diametrical compression", *Int. J. Rock Mech. Min. Sci*., **104**, 71-76

Dong, W., Wu, Z., Zhou, X., Wang, N. and Kastiukas, G. (2017), "An experimental study on crack propagation at rock-concrete interface using digital image correlation technique", *Eng. Fract. Mech*., **171**, 50-63.

Erarslan, N. and Williams, D.J. (2012a), "Mechanism of rock fatigue damage in terms of fracturing modes", *Int. J. Fatigue*, **43**, 76-89.

Erarslan, N. and Williams, D.J. (2012b), "The damage mechanism of rock fatigue and its relationship to fracture toughness of rocks", *Int. J. Rock Mech. Min. Sci*., **56**, 15-26

Fishman, Y.A. (2009a), "Features of shear failure of brittle materials and concrete structures on rock foundations", *Int. J. Rock Mech. Min. Sci*., **45**(6), 976-92.

Fishman, Y.A. (2009b), "Stability of concrete retaining structures and their interface with rock foundations", *Int. J. Rock Mech. Min. Sci*., **46**(6), 957-966.

Granrut, M., Simon, A., Dias, D. (2019), "Artificial neural networks for the interpretation of piezometric levels at the rock-concrete interface of arch dams", *Eng. Struct*., **178**, 616-634.

ISRM (1978), "Suggested methods for determining the tensile strength of rock materials", *Int. J. Rock Mech. Min. Sci.*

Geomech. *Abstr*., **15**, 99-103.
Jayakody, S., Gallage, C. and Kumar, A. (2014), "Assessment of recycled concrete aggregates as a pavement material", *Geomech*. *Eng*., **6**(3) 235-248.
Kodikara, J.K. (1989), "Shear behaviour of rock concrete joints and side resistance of piles in weak rock", Ph.D. Thesis, Monash University, Melbourne, Australia.
Komurlu, E., Kesimal, A. and Hasanpour, R. (2015), "In situ horizontal stress effect on plastic zone around circular underground openings excavated in elastic zones", *Geomech*. *Eng*., **8**(6), 783-799.
Liu, Y., Dai, F., Dong, L., Xu, N. and Feng, P. (2018), "Experimental investigation on the fatigue mechanical properties of intermittently jointed rock models under cyclic uniaxial compression with different loading parameters", *Rock Mech*. *Rock Eng*., **51**(1), 47-68
Liu, Y., Dai, F., Fan, P., Xu, N. and Dong, L. (2017a), "Experimental investigation of the influences of joint geometric configurations on the mechanical properties of intermittent jointed rock models under cyclic uniaxial compression", *Rock Mech*. *Rock Eng*., **50**(6), 1453-1471
Liu, Y., Dai, F., Zhao, T. and Xu, N. (2017b), "Numerical investigation of the dynamic properties of intermittent jointed rock models subjected to cyclic uniaxial compression", *Rock Mech*. *Rock Eng*., **50**(1), 753-765
Plesha, M.E. (1987), "Constitutive models for rock discontinuities with dilatancy and surface degradation", *Int*. *J*. *Numer*. *Anal*. *Meth*. *Geomech*., **11**(4), 345-62.
Prost, C.L. (1998), "Jointing at rock contacts in cyclic loading", *Int. J. Rock Mech. Min. Sci*.*Geomech. Abstr*., **25**(5), 263-272.
Qiu, X., Plesha, M.E., Huang, X. and Haimson, B.C. (1993), "An investigation of the mechanics of rock joints-Part II Analytical investigation", *Int. J. Rock Mech. Min. Sci*. *Geomech. Abstr*., **30**(3), 271-287.
Sukplum, W. and Wannakao, L. (2016), "Influence of confining pressure on the mechanical behaviour of Phu Kradung sandstone", *Int*. *J*. *Rock Mech*. *Min*. *Sci*., **86**, 48-54
Xu. J., Li, S., Tao, Y., Tang, X. and Wu, X. (2009), "Acoustic emission characteristic during rock fatigue damage and failure", *Proc*. *Earth Planet*. *Sci*., **1**(1), 556-559.
Yang, Z., Lo, S. and Di, C. (2001), "Reassessing the joint roughness coefficient (JRC) estimation using Z2", *Rock Mech*. *Rock Eng*., **34**(3), 243-51
Yang, Z.J. and Deeks, A.J. (2007), "Fully-automatic modeling of cohesive crack growth using a finite element-scaled boundary finite element coupled method", *Eng*. *Fract*. *Mech*., **74**, 2547-73.
Zhao, W., Chen, W. and Zhao, K. (2018), "Laboratory test on foamed concrete-rock joints in direct shear", *Constr*. *Build*. *Mater*., **173**, 69-80.
Zhu, H.H., Yin, J.H., Dong, J.H. and Zhang, L. (2010), "Physical modelling of sliding failure of concrete gravity dam under overloading condition", *Geomech*. *Eng*., **2**(2), 89-106.

CC